OPEN ACCESS

Scholars International Journal of Chemistry and Material Sciences

Abbreviated Key Title: Sch Int J Chem Mater Sci
ISSN 2616-8669 (Print) |ISSN 2617-6556 (Online)
Scholars Middle East Publishers, Dubai, United Arab Emirates
Journal homepage: http://saudijournals.com/sijcms/

Original Research Article

Morphology and Study the Crystal Chemistry of a Novel Ternary Mixed Valence $Bi_{1.52}Co_{2.52}Zr_{0.751}N_{0.641}O_{8.12}$ Oxide Orthorhomic Crystal Structure by *Ab Initio* Method via Powder XRD

Yuv Raj Sahu, Parashuram Mishra*

Bioinorganic and Materials Chemistry Research Lab, Tribhuvan University, M.M.A.M. Campus, Biratnagar, Nepal

DOI: 10.36348/sijcms.2020.v03i07.002 | **Received:** 06.09.2020 | **Accepted:** 14.09.2020 | **Published:** 25.09.2020

***Corresponding author:** Parashuram Mishra

Abstract

A novet crystal stucture has been synthesised and solved the scrystal structure by ab intio method via powder XRD and refined by Rietveld methos .The rfined values are $Bi_{1.52}Co_{2.52}N_{0.641}O_{8.12}Zr_{0.751,}$ Formula weight 673.60, Crystal system orthorhombic, Space group *P* 2 2 21 (no. 17) Unit cell dimensions, *a* = 15.5850 Å, *b* = 15.2053 Å,*c* = 15.3691 Å,Cell volume 364.209 $Å^3$,Z=4,Density=1.228 g/cm^3 GOF=0.012, Rp=0.1221, Rw=0.1443. The metal framework of the compound was solved in this investigation via direct methods from hk0 precession electron diffraction intensities recorded with a Philips EM400 at 100 kV. A subsequent (kinematical) least-squares refinement with electron intensities yielded slightly improved co-ordinates for the 11 heavy atoms in the structure. Chemical analysis of several crystallites by EDX is in agreement with the formula are $Bi_{1.52}Co_{2.52}N_{0.641}O_{8.12}Zr_{0.751,}$ Moreover, the structure was independently determined by Rietveld refinement from X-ray powder data obtained from a multi-phasic sample. It has been solved using a *ab intio* techniques based on minimum cation-cations distances and refined with room temperature powder dif fraction data. Least squares refinement of the structure of $Bi_{1.52}Co_{2.52}N_{0.641}O_{8.12}Zr_{0.751,}$ using 70 integrated intensities containing contributiobs form 103 reflections leads to the refinement values.The morphological study the synthesized oxide by SEM and TEM.

Keywords: Powder, diffraction, orthorhombic, cell dimension, crystal system.

INTRODUCTION

Transition and nontransition metal oxide containing mixed valence continue to be the subject of intensive research due to their potential uses as prospective materials for different applications related to their specific properties such as ionic conductivity, piezoelectricity and semi conductivity. Many binary and ternary platinum oxides have already been chemically and structurally studied. Insulator, semiconductor, or metallic conductor platinum oxides have been reported. They can be classified in two groups based on the valence state and the environment of the platinum cations: the first constrains divalent or partially oxidized platinum in planar coordination and the second fully oxidized tetravalent platinum in octahedral coordination [1]. The first group of mixed-valence compounds includes cited oxide which owes its high conductivity to columnar stacks of Bi_2O_3 ZrO_2 and Co_2O_3 groups extending along all three main crystallographic directions with short Bi-Zr-Co distances. Materials with pronounced twinning or new compounds that only exist as part of a complex multi-phase powder sample are thus extremely difficult to treat with this standard method for structure determination. It should be noted that these problem cases also include many technologically relevant products such as small precipitates in a metallic matrix, catalysts, pharmaceuticals, pigments and thin films, which a priori exist only in small quantities or rarely grow as large crystals. Hence, ample motivation exists to develop alternative approaches capable for structural analysis of extremely small volumes and crystallites. However, the only real alternative to X-rays is fast electrons, since their interaction with matter is several orders of magnitude stronger than that of X-rays. Electron diffraction structure analysis (EDSA) makes it, thus, possible to obtain structural information at the atomic level even for the steadily growing number of nanocrystalline materials. On the other hand, structure analysis with electron data is rarely straightforward and fully automated, as it is the case with X-ray data. In particular, the non-kinematical nature of the diffracted intensities is a great concern for structure analysis with

electron diffraction data and has hindered EDSA from becoming very popular since its foundation in Russia more than 65 years ago. While a large number of light-atom structures have been investigated by electron diffraction in the past [1-4], it has only succeeded in a few cases to solve structures with heavier atoms directly from X-ray diffraction spot patterns. In order to avoid these problems, an alternative approach was developed for such non-light-atom structures. This approach exploits the low-order structure factor phases extracted from high resolution electron microscopy microscopy (HREM) images, to assign phases to the higher-order electron diffraction amplitudes [5-9]. In the most favourite case when the scattering power of the elements in the structure is not too different, the complete structure can be solved from HREM images and subsequently refined with electron diffraction data [10, 11]. Despite such hybrid methods proved very efficient, it is still highly desirable to also develop methods which allow solving heavy-atom structures directly from the measured electron diffraction amplitudes. As mentioned earlier, the non-kinematical (dynamical) nature of the electron intensities is the main concern in this endeavour because its influence on the diffracted intensities is very difficult to control in the diffraction experiment. However, today it is generally believed that the precession electron diffraction method, developed in the early 1990s by Vincent and Midgley [12], is the most promising way out from this quandary. In the precession method, a small focussed or parallel electron beam is scanned at a constant angle around the optic axis to produce a hollow-cone illumination of the sample. Those electron beams leaving the specimen exit-plane are then descanned in such a way that a that a stationary spot diffraction pattern is formed. Thus, this method is, in principle, equivalent to the precession technique known from X-ray crystallography, where a crystal is turned (tilted) through a small angle about an axis perpendicular to the (stationary) beam [13]. Due to this geometry, the electron diffraction pattern consists of many reflections far out in reciprocal space with intensities that are integrated over the excitation error. The most important effect for quantitative work is, however, that this integration considerably limits the non-systematical dynamical interactions which are most pronounced under on-zone axis conditions [14-16]. To our knowledge, the precession method has so far been used to determine the previously unknown structures of $Bi_{1.52}$ $Co_{2.52}$ $Zr_{0.751}$ $N_{0.641}$ $O_{8.12}$ and obtained from data obtained at 300 kV. Several heavy atom oxides like Er2Ge2O7 [17], MgMoO4 [18], Mg3V2O8, and La4Cu3MoO12 [20] have recently been used to check the potential of the precession method for structure determination. Inspired by these results, we started to try an ab initio structure determination of the complex heavy-atom structure $Bi_{1.52}$ $Co_{2.52}$ $Zr_{0.751}$ $N_{0.641}$ $O_{8.12}$ from 100 kV precession electron data, because all attempts to solve this or related heavy-atom oxides with tunnel structure directly from X-ray diffraction. In this context, it should be noted that a Lorentz correction primarily accounts for the method which is used to collect the intensities and should be independent of the type of the investigated sample (single crystal or polycrystalline material). This paper is described morphology and crystal structure of cited oide by powder XRD followed by *ab initio* method.

MATERIALS AND METHODS

All chemicals used were analytical grade and obtained from SimaAldrich. A polycrystalline sample of $Bi_{1.52}$ $Co_{2.52}$ $Zr_{0.751}$ $N_{0.641}$ $O_{8.12}$ was synthesized by a standard solid state reaction using a mixture of high purity reagents of $Zr(NO_3)_4$,CoCl3 and Bi_2O_3 as starting materials in the molar ratio of 1:1:3. The mixture was ground carefully, homogenized thoroughly with methanol (99%) in an agate mortar and pastel then packed into an alumina crucible and calcined at 1000°C in air for 10h with several intermediate grindings [6]. Finally the product was pressed into pallets and sintered at 100 K/h. Powder X-ray diffraction (XRD) spectra shown in Figure-1 and data were collected at room temperature in the angular range of2 θ =10 to 80 with scan step width of 0.02° and a fixed containing time of 15 s using Philips powder diffractometer with graphite monochromatic CuKa radiation. The powder was rotated during the data collection to minimize preferred Orientation effect if any. The program TREOR in CRYSFIRE was used to index the powder pattern which give orthorhombic cell system. SIRPOW92 was used to locate the positional parameters of constituent atoms. The full pattern is fitting and peak decomposition in the space group P2222 using check cell program. The structural parameters were refined by the Rietveld method using the JANA program which gave Rwp = 0.0354 Rp= 0.0249 and GOF = 1.62. The density is determined by Archimedes principle. The morphology of titled compound was determined using the electrical studies, the measurements were preceded by a pretreatment of the sample in order to reduce the mean particle size of the obtained powder after these treatments, the sample achieved about 85% of the theoretical density with the final diameter of 8 mm and thickness of 2 mm. The relative density of the sample before the mechanical grinding was 79 %. Platinum electrodes were connected to the two faces of the pellet via a platinum paste to keep good electric contacts [10].

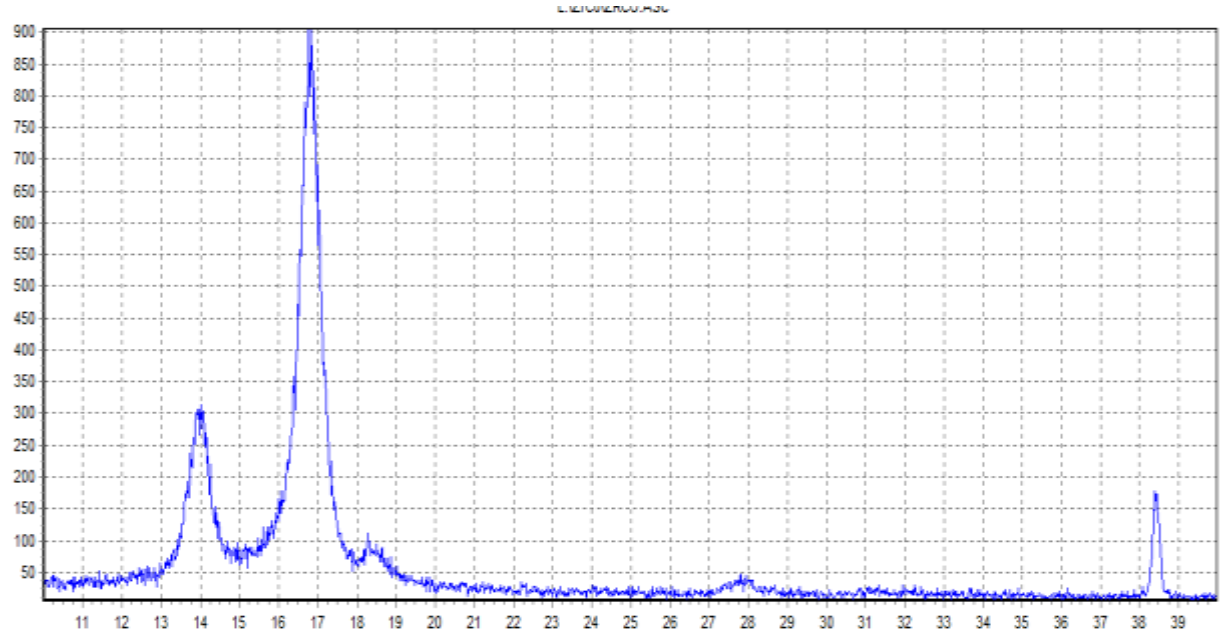

Fig-1: Powder XRD spectra of $Bi_{1.52}$ $Co_{2.52}$ $N_{0.641}$ $O_{8.12}$ $Zr_{0.751}$

Impedance spectroscopy measurements were carried out using a Hewlett-Packard 4192a Impedance Analyzer. The impedance spectra were recorded in the 5 Hz-13 MHz frequency range. Electrical conductivity measurements of representative $Bi_{0.876}$ $Mn_{0.541}$ $Zr_{0.125}$ $N_{0.231}$ $O_{1.567}$ were carried out by complex impedance spectroscopy with a 1174 Solartron frequency response analyzer coupled to a 1286 Solartron electrochemical interface. Pellets of about 14 mm diameter and 1 mm thickness were prepared by cold pressing of a mechanically activated powder mixture with the composition $Bi_{1.52}$ $Co_{2.52}$ $Zr_{0.751}$ $N_{0.641}$ $O_{8.12}$.To form the phase, the pellets were heated at 7003C during 12 h and slowly cooled to room temperature. This synthesis method was employed to improve the ceramic quality, as it has been shown for other materials. The formed phases and crystallinity were studied by X-ray powder diffraction. Platinum electrodes were deposited on the two faces by sputtering, and measurements were carried out in the temperature range 200-1100^{0}C, at steady temperatures, with pellets under airflow the frequency range was fixed. The morphology was study by SEM and TEM.

RESULTS AND DISCUSSIONS

Synthesis

$Bi_{1.52}$ $Co_{2.52}$ $Zr_{0.751}$ $N_{0.641}$ $O_{8.12}$ was synthesized by a typical high-temperature solid state reaction. The difficulty to obtain a pure phase is because it is an intermediate and metastable phase during the high temperature annealing process of Bi_2O_3-$CoCl_3$-$Zr(NO_3)_4$ system. Two deciding factors of the formation of phase 1 are: the starting cationic ratio and annealing time. Even though phase 1 forms with a suitable starting cationic ratio, the relative percentage between the phases varies against the annealing time. In this work, we focused on two samples A and B, which both contain a large content of phase 1. The starting ratios for A and B are the same, Bi2O3: CoCl3 : Zr(NO3)4 = (molar ratio is 1 : 1 : 3). For A, a well-crystallized parent phase mullite- $Bi_{1.52}$ $Co_{2.52}$ $Zr_{0.751}$ $N_{0.641}$ $O_{8.12}$ formed during the first heating step, and phase 1 appeared (monitored by PXRD) after being heated at room temperature for 120 h and the percentage kept increasing with further heating at 1025 °C and reached the maximum at about 840 h. In the meantime, the percentage of mullite- $Bi_{1.52}$ $Co_{2.52}$ $Zr_{0.751}$ $N_{0.641}$ $O_{8.12}$ decreased. During this process, the sample A kept losing weight to 0.56 g, due to the volatilization of bismuth. So, 0.1000 g of Bi2O3 was added to compensate for the loss of Bi. After another 300 h of heating, the PXRD data for the structure determination were collected After a further 40 h of heating at 1025 °C, high quality PXRD data were collected. Twenty-two different starting cationic ratios were attempted and there showed a large tolerance for the formation of phase 1. The cationic ratio in phase 1 was estimated by energy-dispersive X-ray spectroscopy (EDS) to be Bi :Zr : Co = 1.5(1) : 1.0(2) : 6.0(2). If started with an exact cationic ratio from EDS, after 24 h annealing at 1000 °C, only a small amount of multiphase appears. Apparently, as a kinetics process, the phase diagram rules are not applicable to this case, and the synthesis process is mainly empirical.

STRUCTURE SOLUTION FROM SAMPLE $Bi_{1.52}$ $Co_{2.52}$ $Zr_{0.751}$ $N_{0.641}$ $O_{8.12}$

X-Ray powder diffraction and Rietveld refinements:

X-Ray powder diffraction (XRD) patterns were collected on a PANalytical X'Pert-MPD diffractometer using graphite-monochromated Cu-Kα radiation. The data were collected at 40 kV, 30 mA with a step size of 0.02° in the 2θ range of 5–80°. Rietveld refinements of the XRD patterns were performed using JANA package. The backgrounds were fit with

Chebyschev function, and Bragg-Brentano was selected as diffractometer type. Lattice constants, instrument parameters, atomic coordinates, thermal parameters, and peak profile functions were refined in order to achieve a simulated diffraction pattern that matched the experimental data. The completed refinements provided phase quantification and lattice parameter determination. The observed, difference and calculated patterns of the newly synthesized novel oxide obtained by Rietveld refinement has been shown in Fig-1. The structure in packing from shown in Figure-2. In the structure Bi is bonded with Co-Zr bonded with Bi-O,-Co with O) each forming closed type structure. The bonding between different constituent atoms has been discussed in more details in Table-2. In conclusion, the structure of $Bi_{1.52}$ $Co_{2.52}$ $N_{0.641}$ $O_{8.12}$ $Zr_{0.}$been solved by the *ab initio* approach using powder X-ray diffraction data. $Bi_{1.52}$ $Co_{2.52}$ $N_{0.641}$ $O_{8.12}$ $Zr_{0.751}$was found to crystalline in orthorhombic crystal system with space group P-1 which displays an unusual spiral chain structure along the c-axis and packing form on three-dimensional axis. The data were analyse Diamond package with help of CIF file. Rietveld refinement of triclinic crystal system $Bi_{1.52}$ $Co_{2.52}$ $N_{0.641}$ $O_{8.12}$ $Zr_{0.}$ against XRD data for structural determination proved difficult, due to a combination of preferred orientation of the plate-like crystallites in flat-plate geometry[13].In other words, the extracted peak intensities for phase 1 could be reliable. Note that if the relative intensities differed a lot from the simulated patterns of the known phases, additional manual partitioning of those overlapping peaks would be necessary to get reliable intensities for the unknown phase After considering the multiplicity and Lorentz-polarization correction, the intensities of multi phase 1 were used for the structure solution as below. Moreover, the reflection conditions indicated possible space groups P2222. The initial structure model was obtained using a charge flipping algorithm with the program Superflip.8 from Jana package [21]. Random phases were used at the beginning of the charge-flipping iteration, and overlapping peaks were re-partitioned using a histogram match to improve the convergence. The iteration converged with an R factor of 15% and the final electron density shows a P2222 symmetry with a 5% error. The program of EDMA was then used to automatically assign atomic positions. Four unique heavy atomic positions were found and the heaviest one was assigned as Bi while the others were considered as Bi nd U Due to the existence of heavy atoms, all oxygen positions were ambiguous in the electron density map of this stage [22]. To locate the oxygen atoms, a Monte-Carlo based simulated annealing process with the program TOPAS was applied. For each annealing process, various atomic coordinates were randomly assigned as the initial positions of the oxygen atoms [23]. The annealing process was restarted after finding a few oxygen positions, until all oxygen positions were found to be reasonable.

The PXRD pattern of sample $Bi_{1.52}$ $Co_{2.52}$ $N_{0.641}$ $O_{8.12}$ $Zr_{0.}$is good quality obtained and polycrystalline phases can be identified as spinel-Bi2O3 –CoCl3 and Zr(NO3)4. The rest of the strong peaks can be indexed by the orthorhombic unit cell with a = 15.5850 Å, b = 15.2053 Å,c = 15.3691 Å,Cell volume 364.209 $Å^3$,Z=4, Density=1.228 g/cm^3 GOF=0.012,Rp=0.1221,Rw=0.1443 . A few very weak peaks related to the mullite- $Bi_{1.52}$ $Co_{2.52}$ $Zr_{0.751}$ $N_{0.641}$ $O_{8.12}$ can be also observed, which were ignored during the structure determination. The PXRD pattern from sample A was chosen to extract reflection intensities of phase 1. Only multi phase (phase, $Bi_{1.52}$ $Co_{2.52}$ $Zr_{0.751}$ $N_{0.641}$ $O_{8.12}$) were included for the Le Bail fitting using Jana 2006 [7]. All peak intensities of Bi2O3 –CoCl3 and Zr(NO3)4 in the output were compared with the simulated intensities calculated from reported structures. Note that if the relative intensities differed a lot from the simulated patterns of the known phases, additional manual partitioning of those overlapping peaks would be necessary to get reliable intensities for the unknown phase. After considering the multiplicity and Lorentz-polarization correction, the intensities of phase were used for the structure solution as below and the crystallographic data and atomic coordinate are given in Table 1 and 2 which are given the proper position of tenari metal oxide (cited). Moreover, the reflection conditions indicated possible space groups P2222 the initial structure model was obtained using a charge flipping algorithm with the program Superflip.8 Random phases were used at the beginning of the charge-flipping iteration, and overlapping peaks were re-partitioned using a histogram match to improve the convergence. The iteration converged with an Rfactor of 15% and the final electron density shows a P2222 symmetry with a 5% error. The program of EDMA was then used to automatically assign atomic positions [9]. Four unique heavy atomic positions were found and the heaviest one was assigned as Bi, while the others were considered as Bi/Zr/Co. Due to the existence of heavy atoms, all oxygen positions were ambiguous in the electron density map of this stage. To locate the oxygen atoms, a Monte-Carlo based simulated annealing process with the program TOPAS was applied. For each annealing process, various atomic coordinates were randomly assigned as the initial positions of the oxygen atoms. The annealing process was restarted after finding a few oxygen positions, until all oxygen positions were found to be reasonable the valence position is determined by using SIR-92 computer program. The structure mode of the cited oxide shown in Figure-3 and projected model shown in Figure-4.

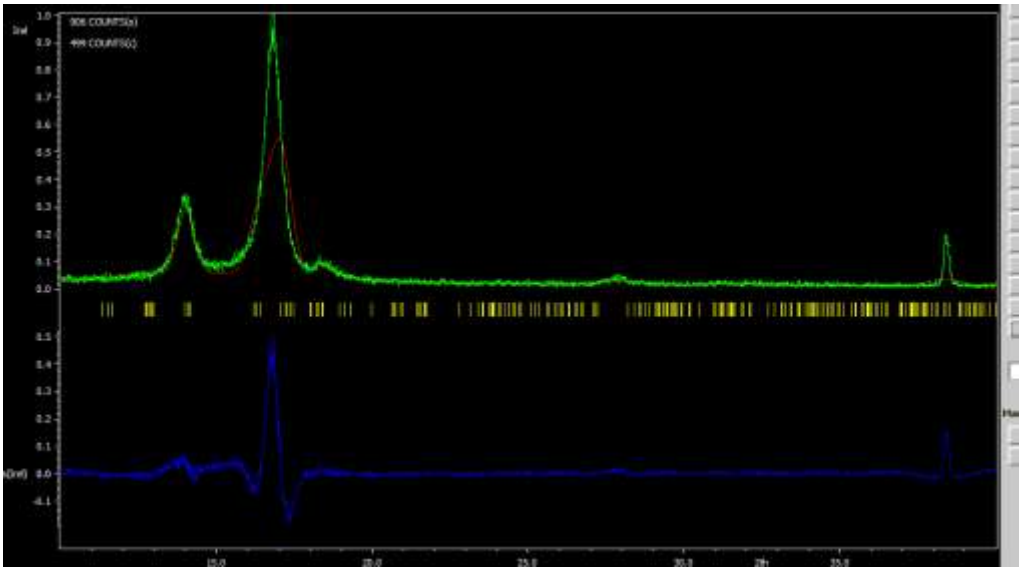

Fig-2: Graphical representation of the result from Rietveld refinement with X-ray powder data. Vertical bars indicate positions of the Bragg reflections for Bi0.5 Mn0.125 Mo0.5 O0.67 U0.32dots mark the observed intensities and the solid line gives the calculated intensity curve. The deviations between the observed and the calculated intensities from the refined model are shown by the difference plot in the lower part of the diagram.

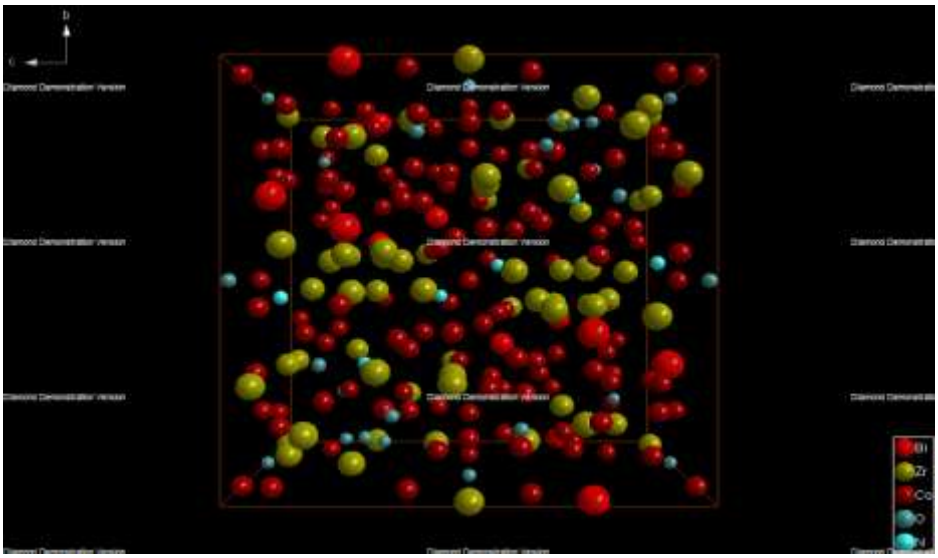

Fig-3: Structure of $Bi_{1.52}$ $Co_{2.52}$ $N_{0.641}$ $O_{8.12}$ $Zr_{0.751}$

Table-1: Crystallographic data

Creation method	
Jana 2006 Version : 25/10/2015	
Crystal Data	
Formula sum	$Bi_{1.52}$ $Co_{2.52}$ $N_{0.641}$ $O_{8.12}$ $Zr_{0.751}$
Formula weight	673.60
Crystal system orthorhombic	
Space group	*P* 2 2 21 (no. 17)
Unit cell dimensions	*a* = 15.5850 Å
	b = 15.2053 Å
	c = 15.3691 Å
Cell volume	3642.09 $Å^3$
Z	4
Density, calculated	1.2347g/cm^3
Meas.density	1.228 g/cm^3
Pearson code	oP230
Formula type	N3O4P11Q31R66
Wyckoff sequence	$e^{53}d^2c^2b^2a^3$
Index	- 4≤h≤1 ,-1≤k≤0,0≤l≤2

Table-2: Atomic coordinates and isotropic displacement parameters (in Å ^{2})

Atom	Wyck.	x	y	z	U
Bi1	2*c*	0	0.38370	1/4	0.0380
Bi2	4*e*	-0.06820	0.30790	0.09030	0.0380
Bi3	2*c*	0	0.01350	1/4	0.0380
Zr1	4*e*	0.46330	0.55170	-0.16300	0.0380
Zr2	4*e*	-0.01400	0.15370	-0.16510	0.0380
Zr3	4*e*	0.31010	0.26250	-0.03720	0.0380
Zr4	4*e*	-0.29260	-0.04670	0.23680	0.0380
Zr5	4*e*	-0.08830	0.25600	-0.04520	0.0380
Zr6	2*a*	0.05070	0	0	0.0380
Zr7	4*e*	0.06330	0.29110	-0.19290	0.0380
Zr8	4*e*	0.10390	0.26050	-0.03510	0.0380
Zr9	4*e*	0.33500	0.47590	-0.10300	0.0380
Zr10	4*e*	0.33620	0.09800	0.13020	0.0380
Zr11	4*e*	0.28840	0.14440	0.26110	0.0380
Zr12	4*e*	-0.04700	0.41900	0.11540	0.0380
Zr13	4*e*	0.28660	0.47050	-0.26330	0.0380
Zr14	4*e*	-0.38900	-0.05400	0.08210	0.0380
Zr15	4*e*	0.36360	0.56500	-0.28650	0.0380
Zr16	4*e*	0.22470	0.57060	-0.18600	0.0380
Co1	4*e*	-0.06790	0.55590	0.23360	0.0380
Co2	4*e*	-0.22250	0.41590	0.09590	0.0380
Co3	4*e*	-0.20020	0.18470	0.08900	0.0380
Co4	4*e*	0.31990	0.29810	0.14950	0.0380
Co5	4*e*	-0.19350	0.28600	0.22950	0.0380
Co6	4*e*	0.03460	0.12570	0.10500	0.0380
Co7	2*b*	-0.49160	1/2	0	.0380
Co8	4*e*	0.42350	0.16380	-0.14070	0.0380
Co9	4*e*	-0.28770	0.06680	0.09050	0.0380
Co10	4*e*	-0.37960	-0.19150	0.16330	0.0380
Co11	4*e*	0.35650	0.32700	-0.13790	0.0380
Co12	4*e*	0.38920	0.61070	-0.03250	0.0380
Co13	4*e*	-0.38890	0.23610	0.05500	0.0380
Co14	4*e*	-0.10140	0.02280	-0.08740	0.0380
Co15	4*e*	-0.26650	-0.14100	0.07870	0.0380
Co16	4*e*	0.54900	0.63820	0.11130	0.0380
Co17	4*e*	0.41210	0.06450	0.24230	0.0380
Co18	4*e*	0.03930	0.38280	-0.03390	0.0380
Co19	4*e*	-0.27640	0.27260	-0.02530	0.0380
Co20	4*e*	0.35750	0.24340	0.32350	0.0380
Co21	2*a*	-0.24540	0	0	0.0380
Co22	4*e*	0.38080	0.22450	0.04650	0.0380
Co23	4*e*	-0.35640	0.40970	0.07170	0.0380
Co24	4*e*	-0.17540	-0.00470	0.36680	0.0380
Co25	4*e*	-0.15030	0.43550	-0.05140	0.0380
Co26	4*e*	0.10300	0.32050	0.09860	0.0380
Co27	4*e*	0.19290	0.36030	-0.15540	0.0380
Co28	4*e*	0.20630	0.22980	0.12110	0.0380
Co29	4*e*	0.47780	0.10120	0.22540	0.0380
Co30	4*e*	0.21900	0.11900	-0.00130	0.0380
Co31	4*e*	-0.24570	-0.18630	0.31220	0.0380
Co32	4*e*	0.47120	0.15160	0.00020	0.0380
Co33	4*e*	0.31300	0.07770	-0.07130	0.0380
Co34	4*e*	-0.06790	0.17680	0.22810	0.0380
O1	4*e*	-0.19530	-0.17630	0.33330	0.0380
O2	2*a*	0.39900	0	0	0.0380
O3	4*e*	0.14840	0.15010	0.11150	0.0380
O4	4*e*	0.82320	0.70100	0.17720	0.0380
O5	2*b*	-0.09020	1/2	0	0.0380
O6	4*e*	0.47790	0.07680	-0.20240	0.0380
O7	2*d*	1/2	0.08320	-1/4	0.0380
N1	4*e*	-0.32640	0.54320	0.07270	0.0380
N2	2*d*	1/2	0.71990	1/4	0.0380

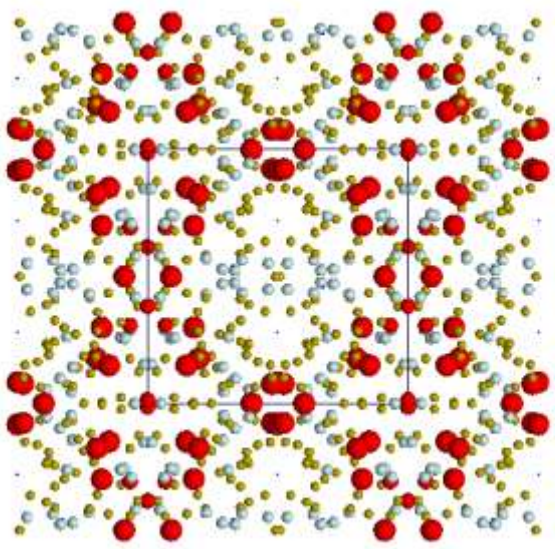

Fig-4: Structure model of $Bi_{1.52}$ $Co_{2.52}$ $N_{0.641}$ $O_{8.12}$ $Zr_{0.751}$ in projection along the short c-axis as obtained from Rietveld refinement with the X-ray powder data

Table-3: Atom1 Aomm2 Atom3 Bond angle

Bi1	Zr12	Zr12	152.518
Bi2	Zr12	Zr5	124.375
Zr1	Zr15	Co12	107.432
	Zr15	Zr9	79.447
	Co12	Zr9	59.573
Zr3	Co22	Co11	119.914
Zr7	Co27	Zr2	139.637
Zr8	Co18	Co26	68.393
Co8	O6	Co32	106.215
O5	Co25	Co25	106.691
	Co25	Zr12	97.081
N1	Co23	Co23	104.018
	Co23	Co16	113.055
	Co23	Co16	83.942

Morphological Study by SEM (Scanning Electron Microscopy)

Scanning electron microscopy (SEM) is giving morphological examination with direct visualization. The techniques based on electron microscopy offer several advantages in morphological and sizing analysis; however, they provide limited information about the size distribution. For SEM characterization, nanoparticles solution should be first converted into a dry powder, which is then mounted on a sample holder followed by coating with a conductive metal, such as gold, using a sputter coater [24]. The sample is then scanned with a focused fine beam of electrons. The surface characteristics of the sample are obtained from the secondary electrons emitted from the sample surface. The morphology of the oxide nanoparticles is shown in Fig-2. From the image, it is clear that the particles were highly agglomerated in nature. The SEM pictures clearly show randomly distributed grains with smaller size. From the SEM analyses, one can conclude the formation of nanoparticles spherical structure. Here it is grown in very high-density and possessing almost uniform spherical shapes. The SEM images for the $Bi_{1.52}$ $Co_{2.52}N_{0.641}$ $O_{8.12}$ $Zr_{0.751}$ shown in Figure-5. All of the binary metal oxides present large aggregations on the top of the nanowire array or nanosheet array. The aggregations are composed of the nanospheres assembled by the well-defined nanowires for the $Bi_{1.52}$ $Co_{2.52}$ $N_{0.641}$ $O_{8.12}$ $Zr_{0.751}$ electrode. It is inferred that the nanosheet morphology and irregular aggregations would prefer to be formed for the $Bi_{1.52}$ $Co_{2.52}$ $N_{0.641}$ $O_{8.12}$ $Zr_{0.751}$ based oxides. The image reveals that the average size of the particles is 25.32 nm. The sample is then scanned with a focused fine beam of electrons. The surface characteristics of the sample are obtained from the secondary electrons emitted [12] from the sample surface. The morphology of the oxide nanoparticles is shown in Fig-2. From the image, it is clear that the particles were highly agglomerated in nature. The SEM pictures clearly show randomly distributed grains with smaller size. From the SEM analyses, one can conclude the formation of nanoparticles spherical structure. Here it is grown in very high-density and possessing almost uniform spherical shapes. The image reveals that the average size of the particles is 25.32 nm.

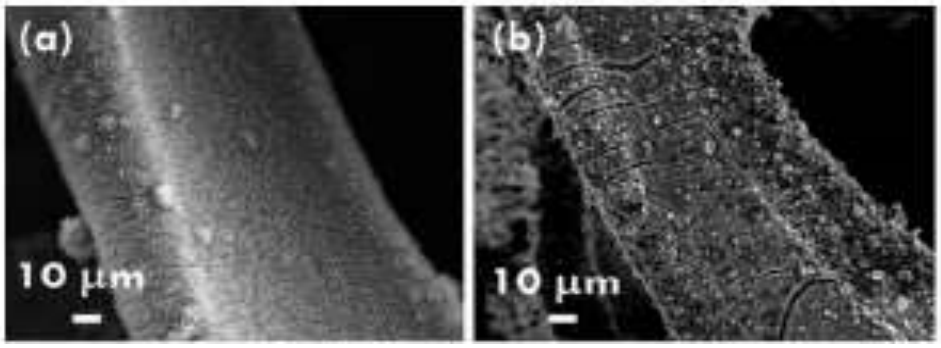

Fig-5: The SEM images for the $Bi_{1.52}$ $Co_{2.52}$ $N_{0.641}$ $O_{8.12}$ $Zr_{0.751}$oxides prepared using the precursor ratio (Bi:Co:Zr) of (a,) 1:2:0.5, (b,) 1:2:1

Electrode Moreover, the ternary metal oxide, the $Bi_{1.52}$ $Co_{2.52}$ $N_{0.641}$ $O_{8.12}$ $Zr_{0.751}$ shows even larger and well-defined nanosheet morphology (Figure-1 (i)) comparing to those for the Bix Zrx Cox electrodes. The larger and well-defined nanosheet morphology for NixCoyMozO is benefit for enhancing the electrochemical performance.

Transmission Electron Microscopy TEM

In order to gain additional insight on crystallographic structure, microstructure, and morphology of the $Na_{24}Bi_4Cs_8$ Cl_{26} samples, we performed TEM and selected area electron diffraction (SAED) on cross-sectional samples of the material. The advantage of these methods over conventional XRD is that they provide spatially resolved structural measurements, which help to elucidate phase-purity and crystallinity of the sample at smaller length scales. A potential drawback is that the material may be damaged during sample preparation via focused-ion beam milling, and that TEM/SAED preparation and analysis can be quite time-consuming procedures. The TEM imaging shown in Figures 7 indicates that the $Na_{24}Bi_4Cs_8$ Cl_{26} layer is polycrystalline, with 80-100 nm sized columnar regions that consist of 10 nm sized crystalline particles surrounded by more disordered material [25]. These TEM observations are consistent with the SEM results is agree with each other. Similar small-grain microstructures have been observed in other novel chloride materials in their initial stages of development. In order to analyze small areas of the sample that were inaccessible via SAED, we performed fast Fourier transforms (FFTs) of several single particles from the high-resolution [26] TEM images (represented in Figure-7. The results of this analysis indicate that crystalline areas of the $Na_{24}Bi_4Cs_8$ Cl_{26} samples are a multiphase phase, and this phase is the same across the several studies regions. Furthermore, the SAED/FFT analysis suggests that $Na_{24}Bi_4Cs_8$ Cl_{26} crystal structure has a small unit cell with low symmetry, consistent with conclusions from the prior XRD analysis good dispersion may be achieved by surface modification of the nanoparticles under appropriate processing parameters. Secondary interactions can occur between certain functional groups attached to the nanoparticle surface and the rubber matrix, wrapping a polymer around the nanoparticle, or by using surfactants. In this sense, a good dispersion degree can be obtained using ultrafine powders with high superficial electric-charge and high surface area. Particles could be identified with nanometric dimensions ($\leq$ 75 nm) and small aggregates ($>$ 85 nm and $\leq$ 100 nm) used in the ceramic phase shown in Figure-5. Sub-micrometric particles (>100 nm) were also found and are associated mainly with particles of the vulcanization system that are larger than the ceramic nanoparticles synthesized [27, 28].

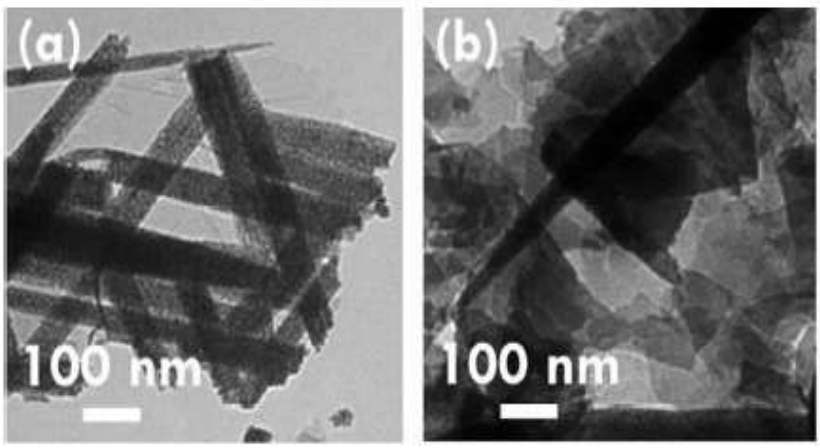

Fig-5: The TEM images for the $Bi_{1.52}$ $Co_{2.52}$ $N_{0.641}$ $O_{8.12}$ $Zr_{0.}$ oxides prepared using the precursor ratio (Bi:Co:Zr) of (a) 1:2:0.5, (b) 1:2:1

CONCLUSIONS

The title compound, $Bi_{1.52}$ $Co_{2.52}$ $N_{0.641}$ $O_{8.12}$ $Zr_{0.}$ has been synthesized as polycrystalline powder by solid-state method. To the present authors' knowledge, our work is the first to uncover the metal framework structure of a large unit cell heavy-metal oxide contained mixed valence with tunnel structure directly from single-projection X-ray diffraction data. To reach this goal, large-angle precession X-ray diffraction intensities have been collected on imaging plates at 100 kV. Processing of the data was performed following the quasi-kinematical approach as outlined elsewhere .Suggested data correction schemes for the geometry of off-axis hollow-cone illumination have been checked, but were not applied because this impaired the quality of the data. Thus, the framework structure of the title compound was solved from uncorrected data with 1A˚ resolution using the direct methods program SIR97. All atoms in the asymmetric unit of the $Bi_{1.52}$ $Co_{2.52}$ $N_{0.641}$ $O_{8.12}$ $Zr_{0.}$ framework were readily found by the program and correctly assigned with their 3D coordinates. A (kinematical) least-squares structure refinement of the heavy-atom positions was carried out with the program JANA using the same hk0 data set. Comparison of the refined co-ordinates for the heavy atoms resulting from Rietveld refinement on X-ray powder data (present study) showed an average agreement for the metal framework structure within 0.09A˚. SEM analysis of several crystallites examined indicate an average chemical composition of this phase according to $Bi_{1.52}$ $Co_{2.52}$ $N_{0.641}$ $O_{8.12}$ $Zr_{0...}$Despite the quality of the available precession X-ray diffraction data proved sufficient for accurate determination of the heavy-atom positions, the data quality did not allow to unambiguously locate the vanadium atoms inside the tunnels nor to reveal the oxygen atoms. Theoretical calculations carried out for the $Bi_{1.52}$ $Co_{2.52}$ $N_{0.641}$ $O_{8.12}$ $Zr_{0.}$ framework structure show that simple formulas for the detectability of light atoms in the presence of heavy atoms can be misleading, since the background noise which results from truncation errors in the Fourier synthesis is not taken into account. Thus, for calculated data with 1A˚ resolution it was found that the heavy atoms appear effectively 7.8 times stronger in the projected map than the oxygen. This explains why it would be very difficult with real data to detect the oxygen and nitrogen positions, in particular if only data from a single zone axis are considered as in the present case. The fact that it was neither possible to detect the oxygen nor the calcium atoms in the structure is a strong indicator that the data from precession X-ray diffraction still contain considerable amounts of dynamical/secondary scattering. This is also displayed by the relatively large R-factors after LS-refinement (15%). From our point of view, the fact that it was possible to determine the heavy-atom positions with high precision even from 100 kV data is yet a great success, because solving these types of heavy-metal framework structures directly from X-ray diffraction data was attempted by several groups for many years, but obviously, without success. Therefore, the present result is a striking example where precession X-ray diffraction reduced dynamical diffraction below the critical limit at which the determination of the structure or, at least, a fundamental part of it is enabled. However, further experiments which address to optimized conditions for detecting the oxygen atoms in heavy-atom structures seem to be necessary. So collection of 3D intensity data are likely more promising to reach this goal, since such extended data sets proved sufficient to detect even the most light atom, oxygen and nitrogen atoms. So from the above discussion we concluded that the structure of cited compound by powder pattern and the particle show nanomaterial can be used in super conductor.

REFERENCES

1. Weirich, T. E., Portillo, J., Cox, G., Hibst, H., & Nicolopoulos, S. (2006). Ab initio determination of the framework structure of the heavy-metal oxide CsxNb2. 54W2. 46O14 from 100 kV precession electron diffraction data. *Ultramicroscopy*, *106*(3), 164-175.
2. Zhou, Z., Palatinus, L., & Sun, J. (2016). Structure determination of modulated structures by powder X-ray diffraction and electron diffraction. *Inorganic Chemistry Frontiers*, *3*(11), 1351-1362.
3. Vu, T. D., Krichen, F., Barre, M., Coste, S., Jouanneaux, A., Suard, E., ... & Goutenoire, F. (2019). Ab Initio Structure Determination of La34Mo8O75 Using Powder X-ray and Neutron Diffraction Data. *Crystal Growth & Design*, *19*(11), 6074-6081.
4. Bimal, K., Parashuram, M. (2020). Synthesis and structure determination of novel mixed valence Pb 0.5 u0.25 zr 1.25 o4.5 by powder xrd obtained from pbco3 -u(co3)2 zr(co3)2 ternary mixed valence oxides. *International journal for research in applied and natural science*. 6(7).
5. Minakshi, M., Mitchell, D. R., Baur, C., Chable, J., Barlow, A. J., Fichtner, M., ... & Ahuja, R. (2019). Phase evolution in calcium molybdate nanoparticles as a function of synthesis temperature and its electrochemical effect on energy storage. *Nanoscale Advances*, *1*(2), 565-580.
6. You, J., Xin, L., Yu, X., Zhou, X., & Liu, Y. (2018). Synthesis of homogeneous CaMoO 4 microspheres with nanopits for high-capacity anode material in Li-ion battery. *Applied Physics A*, *124*(3), 271.
7. Liang, Y., Han, X., Yi, Z., Tang, W., Zhou, L., Sun, J., ... & Zhou, Y. (2007). Synthesis, characterization and lithium-intercalation properties of rod-like CaMoO 4 nanocrystals. *Journal of Solid State Electrochemistry*, *11*(8), 1127-1131.
8. Parashuram, M. (2011). Synthesis, crystal structure determination and ionic properties of

novel BiCa0.5Mg0.5 O2.5 via X- ray powder diffraction data. *Crystal Growth.* 2041(32):2041-204.

9. Bertocco, P., Bolli, C., Bicho, B. A. C., Jenne, C., & Nierstenhöfer, M. C. (2020). Insights into the Structure of Halide-Rich Hydrochloric and Hydrobromic Acid: A Structural and Quantum-Chemical Investigation of the [H 6 X 4 O 2] 2−(X= Cl, Br) Anions. *Journal of Chemical Crystallography*, *50*(2), 69-76.
10. [9]Mah Jebli1 · Abdessalem Badri1 · Mongi Ben Amara1 Journal of Chemical Crystallography. https://doi.org/10.1007/s10870-019-00788-3
11. Tancret, N., Obbade, S., Bettahar, N., & Abraham, F. (1996). Synthesis andab initioStructure Determination from Powder X-Ray Diffraction Data of a New Metallic Mixed-Valence Platinum–Lead Oxide PbPt2O4. *Journal of Solid State Chemistry*, *124*(2), 309-318.
12. Vu, T. D., Krichen, F., Barre, M., Coste, S., Jouanneaux, A., Suard, E., ... & Goutenoire, F. (2019). Ab Initio Structure Determination of La34Mo8O75 Using Powder X-ray and Neutron Diffraction Data. *Crystal Growth & Design*, *19*(11), 6074-6081.
13. Chambrier, M. H., Le Bail, A., Giovannelli, F., Redjaimia, A., Florian, P., Massiot, D., ... & Goutenoire, F. (2014). La10W2O21: An anion-deficient fluorite-related superstructure with oxide ion conduction. *Inorganic chemistry*, *53*(1), 147-159.
14. López-Vergara, A., Porras-Vázquez, J. M., Infantes-Molina, A., Canales-Vázquez, J., Cabeza, A., Losilla, E. R., & Marrero-López, D. (2017). Effect of Preparation Conditions on the Polymorphism and Transport Properties of La6–x MoO12− δ (0≤ x≤ 0.8). *Chemistry of Materials*, *29*(16), 6966-6975.
15. Dubois, F., Goutenoire, F., Laligant, Y., Suard, E., & Lacorre, P. (2001). Ab-Initio determination of La2Mo4O15 crystal structure from x-rays and neutron powder diffraction. *Journal of Solid State Chemistry*, *159*(1), 228-233.
16. Bimal, K. K., & Parashuram, M. (2020). Synthesis and Ab Initio Determination Bi1.256 La0.53 N0.231 O0.521 Zr1.543 Triclinic Structure from Powder X-Ray Diffraction Data. *Sch Int J Chem Mater Sci*, 3(6):6.
17. Charkin, D. O. (2008). Modular approach as applied to the description, prediction, and targeted synthesis of bismuth oxohalides with layered structures. *Russian Journal of Inorganic Chemistry*, *53*(13), 1977-1996.
18. Kresse, G., & Joubert, D. (1999). From ultrasoft pseudopotentials to the projector augmented-wave method. *Physical review b*, *59*(3), 1758-1775.
19. Lü, M., Colmont, M., Kabbour, H., Colis, S., & Mentre, O. (2014). Revised Bi/M layered oxo-sulfate (M= Co, Cu): a structural and magnetic study. *Inorganic chemistry*, *53*(13), 6969-6978.
20. Marzouki, R., Smida, Y. B., Sonni, M., Avdeev, M., & Zid, M. F. (2020). Synthesis, structure, electrical properties and Na+ migration pathways of Na2CoP1. 5As0. 5O7. *Journal of Solid State Chemistry*, *285*, 121058.
21. Ardyanian, M., Moeini, M., & Juybari, H. A. (2014). Thermoelectric and photoconductivity properties of zinc oxide–tin oxide binary systems prepared by spray pyrolysis. *Thin Solid Films*, *552*, 39-45.
22. Chiang, H. Q., Wager, J. F., Hoffman, R. L., Jeong, J., & Keszler, D. A. (2005). High mobility transparent thin-film transistors with amorphous zinc tin oxide channel layer. *Applied Physics Letters*, *86*(1), 013503.
23. Pang, C., Yan, B., Liao, L., Liu, B., Zheng, Z., Wu, T., ... & Yu, T. (2010). Synthesis, characterization and opto-electrical properties of ternary Zn2SnO4 nanowires. *Nanotechnology*, *21*(46), 465706.
24. Jackson, W. B., Hoffman, R. L., & Herman, G. S. (2005). High-performance flexible zinc tin oxide field-effect transistors. *Applied physics letters*, *87*(19), 193503.
25. Phillips, J. M., Cava, R. J., Thomas, G. A., Carter, S. A., Kwo, J., Siegrist, T., ... & Rapkine, D. H. (1995). Zinc- indium- oxide: a high conductivity transparent conducting oxide. *Applied Physics Letters*, *67*(15), 2246-2248.
26. Lim, K. H., Kim, K., Kim, S., Park, S. Y., Kim, H., & Kim, Y. S. (2013). UV–visible spectroscopic analysis of electrical properties in alkali metal- doped amorphous zinc tin oxide thin- film transistors. *Advanced Materials*, *25*(21), 2994-3000.
27. Wang, L., Zhang, X., Liao, X., & Yang, W. (2005). A simple method to synthesize single-crystalline Zn2SnO4 (ZTO) nanowires and their photoluminescence properties. *Nanotechnology*, *16*(12), 2928.
28. Baruah, S., & Dutta, J. (2011). Zinc stannate nanostructures: hydrothermal synthesis. *Science and technology of advanced materials*. 12:18.